frontiers | Frontiers in Earth Science

ORIGINAL RESEARCH
published: 12 May 2022
doi: 10.3389/feart.2022.890171

Tectonic Juxtaposition of Two Independent Paleoproterozoic Arcs by Cenozoic Duplexing in the Arun Tectonic Window of the Eastern Nepalese Himalaya

Rui Li[1,2,3,4]*, *Songjian Ao*[5,4], *Wenjiao Xiao*[1,2,3,4]*, *Karel Schulmann*[6], *Qigui Mao*[1,2,3,4], *Dongfang Song*[5,4], *Zhou Tan*[1,2,3,4], *Hao Wang*[1,2,3,4] and *Saunak Bhandari*[7]

[1]State Key Laboratory of Desert and Oasis Ecology, Xinjiang Institute of Ecology and Geography, Chinese Academy of Sciences, Urumqi, China, [2]Xinjiang Key Laboratory of Mineral Resources and Digital Geology, Urumqi, China, [3]College of Earth and Planetary Sciences, University of Chinese Academy of Sciences, Beijing, China, [4]Innovation Academy for Earth Science, Chinese Academy of Sciences, Beijing, China, [5]State Key Laboratory of Lithospheric Evolution, Institute of Geology and Geophysics, Chinese Academy of Sciences, Beijing, China, [6]Centre for Lithospheric Research, Czech Geological Survey, Prague, Czechia, [7]Department of Mines and Geology, Government of Nepal, Kathmandu, Nepal

OPEN ACCESS

Edited by:
Hanlin Chen,
Zhejiang University, China

Reviewed by:
Shoufa Lin,
University of Waterloo, Canada
Chao Yuan,
Guangzhou Institute of Geochemistry (CAS), China

***Correspondence:**
Rui Li
lirui@ms.xjb.ac.cn
Wenjiao Xiao
wj-xiao@mail.iggcas.ac.cn

Specialty section:
This article was submitted to Structural Geology and Tectonics, a section of the journal Frontiers in Earth Science

Received: 05 March 2022
Accepted: 24 March 2022
Published: 12 May 2022

Citation:
Li R, Ao S, Xiao W, Schulmann K, Mao Q, Song D, Tan Z, Wang H and Bhandari S (2022) Tectonic Juxtaposition of Two Independent Paleoproterozoic Arcs by Cenozoic Duplexing in the Arun Tectonic Window of the Eastern Nepalese Himalaya. Front. Earth Sci. 10:890171. doi: 10.3389/feart.2022.890171

The tectonic evolution of the Himalayan orogenic belt before Cenozoic convergence is important to understand its modern structural framework. There is still controversy regarding the tectonic history of the lower Lesser Himalaya Sequence (LHS) in the frame of the Paleoproterozoic geological record. In this study, integrated analysis of field geology, zircon U-Pb age, Hf isotope, and whole-rock geochemistry was conducted across the LHS and the Main Central Thrust zone in the Arun Valley, eastern Nepal, to address their Precambrian tectonic evolution and the later convergence. Two groups of metasedimentary rocks with different age spectrums of detrital zircons and Hf isotope in the Paleoproterozoic can be distinguished in an imbricated duplexing system in the study area. One group with a maximum depositional age around ca. 1800 Ma has a unimodal detrital zircon pattern and negative zircon ε_{Hf} (t) values ranging from −8.9 to 0.9. These data can be interpreted to reflect the deposition of zircons close to a Japanese-type arc that was isolated from the northern Indian Craton. The other group of calc-silicate rocks and quartzite with multiple peaks of detrital zircons in the Paleoproterozoic show a younger maximum depositional age around ca. 1,600 Ma and variable zircon ε_{Hf} (t) values ranging from −6.7 to 8.8, indicating their deposition in a back-arc basin of an Andean-type arc established on the northern Indian Craton. The geochemistry of an orthogneiss sample dated at 1783 ± 11 Ma indicates high potassium, peraluminous granodiorite protolith emplaced in a volcanic arc or syn-collisional tectonic setting, supporting the existence of the Paleoproterozoic Andean-type arc. We hypothesize that possibly two arc systems developed, respectively, onto and in the proximity of northern Indian Craton in the Paleoproterozoic at the final stages of the Columbia supercontinent formation. These two arcs were juxtaposed either in the Paleoproterozoic or Cenozoic time, and were finally imbricated during the Cenozoic duplexing.

Keywords: Cenozoic duplexing, eastern Nepalese Himalaya, Paleoproterozoic arcs, zircon U–Pb age, zircon Hf

INTRODUCTION

The Himalayan orogenic belt is generated in response to the Cenozoic convergence of the Indian and Eurasian continents, and can be divided into four tectonic units, which are separated by several crustal-scale thrust faults (Gansser, 1964; Yin, 2006). The origin and geometry of these units before convergence played a crucial role in the deformation history of the Himalayan orogenic belt and can be also used to reconstruct the original position of the northern Indian Craton in older supercontinents, such as the Columbia supercontinent (Le Fort, 1975; DeCelles et al., 2000).

The Lesser Himalayan Sequence (LHS) bounded by the Main Central Thrust (MCT) and Main Boundary Thrust (MBT) (Ahmad et al., 1999; Yin, 2006) consists of metasedimentary and meta-volcanic rocks originated along the continental margin of the northern Indian Craton during the Paleoproterozoic (Kohn et al., 2010; Imayama et al., 2018).

There has been controversy as depicted in two different models (passive vs. active continental margin) regarding the tectonic setting of the LHS at the margin of the northern Indian Craton. The passive continental margin model proposed that a series of orthogneiss are regarding continental rifting (Ahmad et al., 1999; Sakai et al., 2013; Larson et al., 2019). This model shows that the rifting magmatism consisted of two episodes: mantle plume-related magmatism during 1.92–1.90 Ga and crustal melting-related magmatism during 1.84–1.74 Ga (Imayama et al., 2018). In contrast, the active continent margin model interpreted the meta-volcanic rocks as a result of a collision event (Regmi and Arita, 2008) or a continental arc (Kohn et al., 2010; Mandal et al., 2016), and proposed that these meta-volcanic rocks were a vestige of the Paleoproterozoic continent arc, while the back-arc extension happened at 1.80 Ga (Mandal et al., 2016).

Cenozoic convergence and intensive shortening of the Himalayan orogenic belt lead to the burial of the rear edge of the LHS. This resulted in the formation of a large duplex system and high-grade metamorphic Greater Himalayan Sequence (GHS) (Yin, 2006; Larson et al., 2010). All the existing Proterozoic models of the northern Indian Craton were mainly based on the investigation of the bottom part of the LHS (Ahmad et al., 1999; Kohn et al., 2010; Sakai et al., 2013; Mandal et al., 2016; Imayama et al., 2018; Larson et al., 2019). However, the rear part of LHS and the frontal part of the northern Indian Craton might have been under-thrusted and hidden beneath the GHS, therefore hampering a full understanding of the tectonic nature of the LHS.

The Arun Valley in eastern Nepal is characterized by a tectonic window where the rear edge of the LHS is exposed, which possibly continues from northern Nepal to southern Tibet of China (Lombardo et al., 1993; Groppo et al., 2007). In this article, we conducted a systematical investigation on the field geology and structural styles along the Arun Valley. The zircons from metamorphic rocks have the texture of core and rim, and we just present new data of U-Pb ages and Hf isotopes of the core of zircons which are interpreted as detrital zircons from metasedimentary rocks and crystallization zircons of orthogneiss across the Arun Valley for the purpose of better understanding their tectonic nature and evolution. Together with the age and whole-rock chemistry of orthogneiss and published data, we propose an updated model of an active continental margin developed in the northern Indian Craton. We propose that the data reflect the development of Paleoproterozoic Japanese-type and Andean-type arcs, followed by a subsequent back-arc extension in the Andean-type arc in 1.6 Ga. In the Himalaya orogenic belt, these two arcs were finally imbricated during the Cenozoic duplexing.

REGIONAL GEOLOGY

The Arun Valley is located in eastern Nepal, following the Arun River that originates from the Ama Drime region of southern Tibet of China (**Figure 1**). The Arun Valley is regarded as a tectonic window in which the erosion of the antiform roof of the GHS has led to the exposition of the rear edge of the LHS (Schelling, 1992; Lombardo et al., 1993; Meier and Hiltner, 1993; Kali et al., 2010). The modern structure of the Arun Valley was controlled by a series of Cenozoic thrusts, which developed as an out-of-sequence system and duplicated the strata within the LHS and Main Central Thrust Zone (MCTZ) (Ambrose et al., 2015; Larson et al., 2015).

Three lithological assemblages have been identified in the Arun Valley from south to north (**Figure 1** and **Figure 2**). The first and structurally deepest assemblage is represented by the Seti Formation consisting of low-grade metasedimentary rocks of quartzite and phyllite (Shrestha et al., 1984). It is exposed in the footwall of the MCT and was possibly deposited at 1,540–1,600 Ma as suggested by Nd isotopic data (Robinson et al., 2001). The second assemblage in the MCTZ is located at the hanging wall of the MCT and beneath the High Himalayan Discontinuity (HHD) and the GHS at the top. It consists of several different sub-groups of rocks (Goscombe et al., 2006; Goscombe et al., 2018): the Himal Group consisting of kyanite/sillimanite bearing schist, the Kushma Formation composed of amphibolite schist and calc-silicate rocks with depositional age at 1,540–1,600 Ma, and the Ulleri orthogneiss forming a thrust sheet of imbricated meta-granitoid rocks dated at ca.1850 Ma and 1780 Ma (Robinson et al., 2001; Kohn et al., 2010). The third lithological assemblage is called the Barun Gneiss, and it lies in the highest structural position of the Arun Valley, which belongs to the GHS. It is represented by a section of granulite facies metamorphic rocks, which contain evidence of medium- to low-pressure partial melting. Some authors also put the MCT in the place of the HHD and suggested that the MCTZ assemblage can be attributed to the LHS (Lombardo et al., 1993; Groppo et al., 2007).

FIELD INVESTIGATION AND SAMPLE DESCRIPTION

A series of thrust sheets was sampled along the Arun Valley (**Figure 2**). Calc-silicate rocks are imbricated with schist, paragneiss, and thick orthogneiss along with clear fault

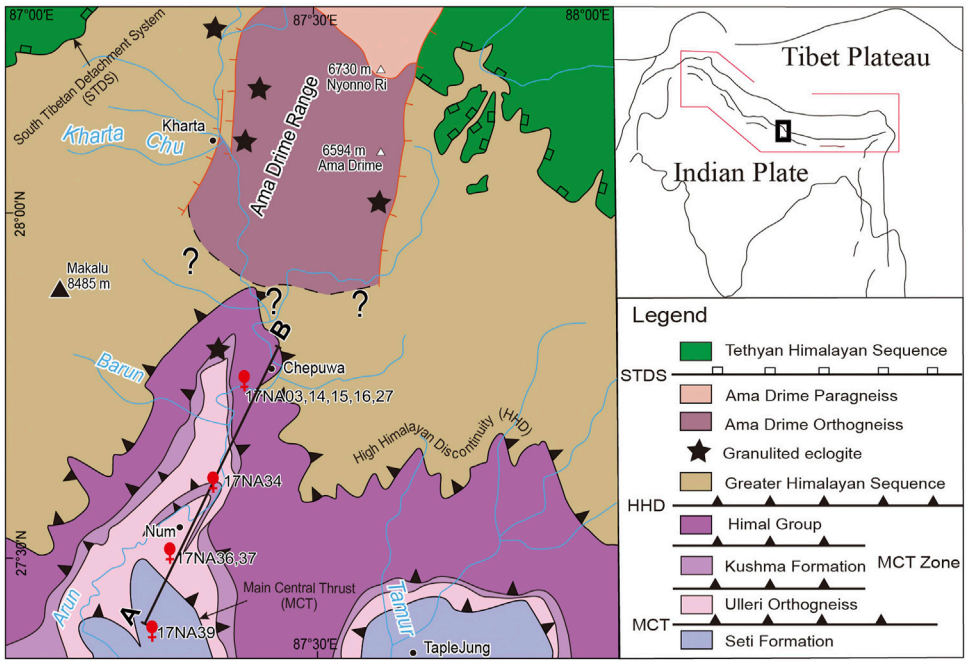

FIGURE 1 | Geological map of northeastern Nepal from the Arun Valley to the Ama Drime Range, modified from the study by Kali et al. (2010) and Goscombe et al. (2018). The Main Central Thrust (MCT) has been mapped in the same location as the Ramgarh Thrust by Goscombe et al. (2018). Profile A–B is in **Figure 2**. STDS, South Tibetan detachment system; HHD, high Himalayan discontinuity.

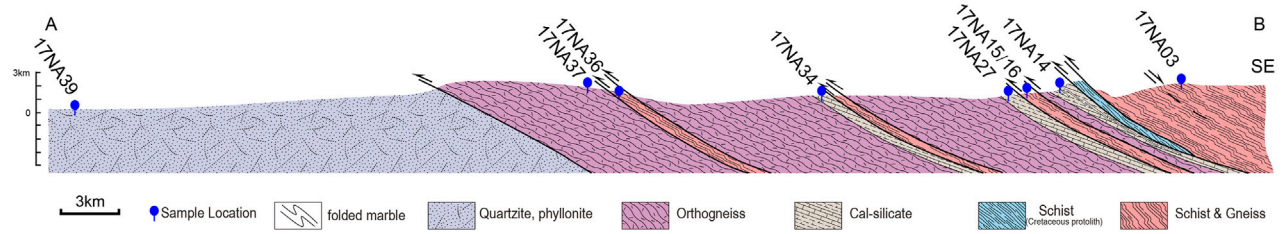

FIGURE 2 | Schematic geological profiles of eastern limb of the Arun Valley. Dashed line represents local detached ductile fault.

contacts (**Figure 3F**). Garnet-bearing sillimanite/kyanite schist sample 17NA03 was collected from a thrust sheet at the Champuwa village in the northernmost part of the valley (**Figures 3A**, **4G**). Below this sheet there is a layer of garnet-free mica schist and a thick layer of calc-silicate rocks (**Figure 2**). The latter rocks associated with layered marble are repetitively exposed in three distinct sheets in the Arun Valley (**Figures 3B–D**). Three calc-silicate rock samples (17NA14, 17NA27, and 17NA34) collected from each sheet consist of calcite, diopside, and biotite (**Figures 4A–C**). Samples 17NA15, 17NA16, and 17NA36 were collected from biotite, muscovite, and garnet-bearing schist and paragneiss (**Figures 4D–G**). Orthogneiss forms the principal bodies of each sheet (**Figures 3E, G**), and sample 17NA37 was collected in the structurally lowermost one. The dominant rock type is formed by highly deformed amphibolite facies orthogneiss with biotite and muscovite aggregates wrapped around the plagioclase augens (**Figure 4H**). In the southernmost part of the Arun Valley, low-grade banded quartzites and phyllites are exposed (**Figure 3H**). Sample 17NA39 was collected from the layered quartzite that was made of finely recrystallized quartz (**Figure 4I**).

ANALYTICAL METHODS

U-Pb Zircon Geochronology Analyses

Zircon grains were separated from ~3 kg samples through a standard procedure of crushing, and heavy-liquid and magnetic separation, and were hand-picked at random. The separated zircon grains were mounted in epoxy resin and polished to expose the grain center. Cathodoluminescent (CL) images were taken with a Nova Nano 450 scanning electron microscope (SEM) at the Institute of Geology and Geophysics, Chinese Academy of Sciences (IGG-CAS). The working

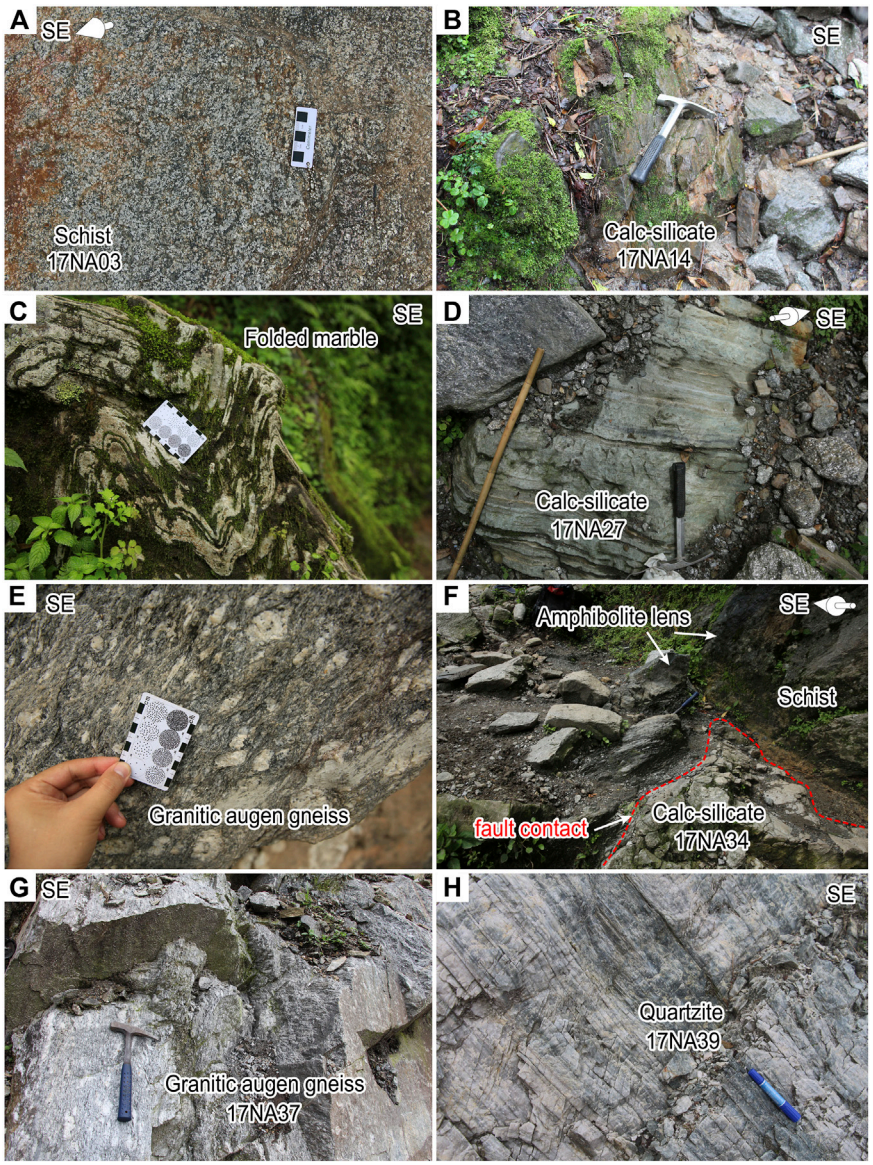

FIGURE 3 | Photographs of the outcrop. **(A)** Garnet schist bears sillimanite and kyanite, **(B)** layered calc-silicate rock contains the interval of metapelites, **(C)** layered marble deforms into the intensive fold, **(D)** layered calc-silicate rocks contain the interval of metapelites, **(E)** mylonite of orthogneiss contains augen of feldspar, **(F)** garnet-schist has a faulted contact with crumpled calc-silicate rocks, **(G)** orthogneiss, and **(H)** layered quartzite.

condition of the CL image was at 15 kV. The internal structures of zircons imaged by CL served to spot the target sites (only cores analyzed in this study) for the U-Pb isotope analyses. In addition, transmitted- and reflected-light microscopic images of zircons were also used to avoid inclusions and fractures during analysis.

U-Pb isotope analyses were undertaken with an Agilent 7500a ICP-MS instrument equipped with a GeoLas 2005 laser system in the State Key Laboratory of Geological Processes and Mineral Resources, China University of Geosciences, Wuhan, China. Detailed instrumental operating settings and data calibrations were described in the study by Liu et al. (2008). The laser spot diameter was 32 μm with a repetition rate of 5 Hz and a fluence of 8 J/cm2. All laser spots were chosen to shoot on the core to avoid the effect of the metamorphic rim. The external standard was zircon 91,500 (Wiedenbeck et al., 1995), two of which were analyzed after every nine zircon grains to correct the U-Pb fractionation and instrumental mass discrimination. Zircon GJ-1 was analyzed as an unknown. Software ICPMSData Cal 10.9 was used for the reduction of data. Standard 91,500 of all analyses yielded the same concordian age, and weighted average $^{206}Pb/^{238}U$ age at 1,062.7 ± 1.4 Ma (n = 275, MSWD = 0.054) is provided in **Supplementary Figure S1** in supplementary. Unknown zircon GJ-1 yielded a concordian age at 595.6 ± 3.0 Ma (n = 79, MSWD = 1.4) and a weighted average $^{206}Pb/^{238}U$ age at 596.3 ± 2.0 Ma (n = 79, MSWD = 2.6) in this study (see **Supplementary Figure S1** in supplementary), which are

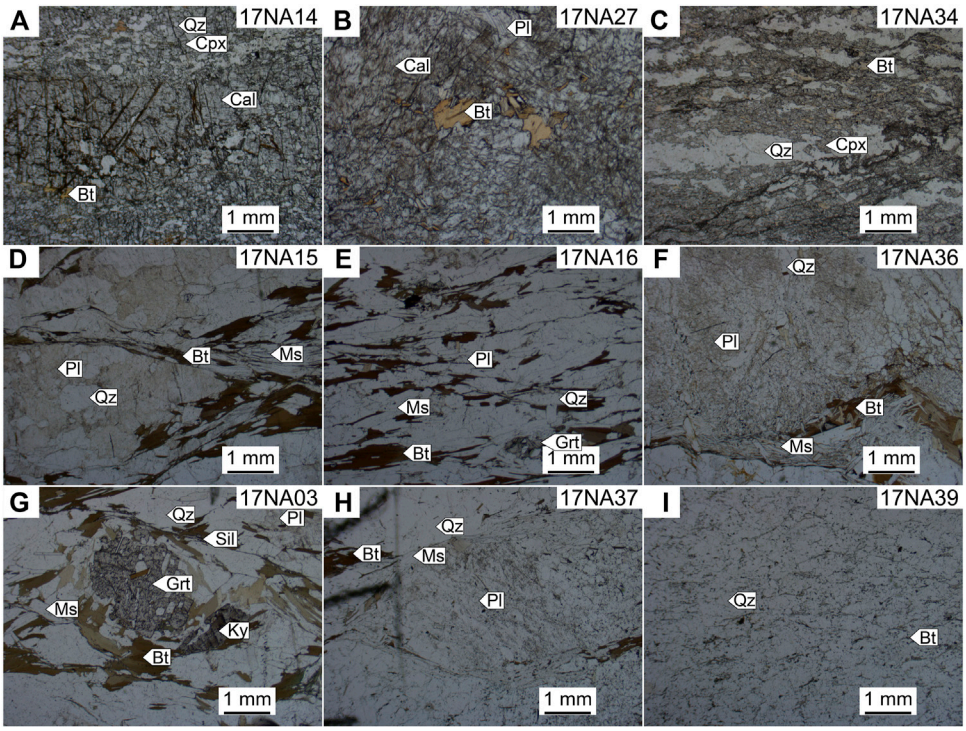

FIGURE 4 | Photographs of samples in the microscope. **(A–C)** Calc-silicate samples contain ferromagnesian minerals such as diopside, indicating protolith contains mafic source; **(D–G)** schist and paragneiss samples contain garnet, plagioclase, biotite, muscovite, and quartz; **(H)** orthogneiss contains Augen plagioclase surrounded by muscovite and biotite; **(I)** quartzite contains quartz and biotite, indicating pelitic cementing of the protolith. Abbreviations follow Whitney and Evans (2010).

consistent with the reference age of 599.8 ± 1.7 Ma (Jackson et al., 2004) (for data of standard, see **Supplementary Table S2** in supplementary). $^{206}Pb/^{238}U$ ages were adopted for zircons younger than 1,000 Ma and $^{207}Pb/^{206}Pb$ ages for ones older than 1,000 Ma. Detrital zircon U-Pb ages with ≥90% concordance were selected to plot kernel density estimation diagrams (KDE) using DensityPlotter software (Vermeesch, 2012). Considering the available data have concordances beyond 90% in this study, the common Pb is not corrected. In orthogneiss sample 17NA37, uncorrected results were plotted on the Wetherill plot, using Isoplot 4.15 (Ludwig, 2008), with an upper intercept age representing the protolith age of this orthogneiss.

Zircon Hf Isotope Analyses

Zircon Hf isotopic measurements were conducted with a *Nu Instruments Nu Plasma II* ICP-MS with a 193-nm *RESOlution LR* laser ablation system (Canberra, Australian) at Nanjing FocuMS Technology Co. Ltd. A laser spot of 50 μm with a 9 Hz repetition rate and a fluence of 4.5 J/cm^2 enabled overlap with the sites of U-Pb dating. Each acquisition incorporated a 20 s background (gas blank), followed by a spot repetition rate of 40 s. Helium (370 ml/min) was applied as a carrier gas to efficiently transport aerosol out of the ablation cell and was mixed with argon (~0.97 L/min) *via* T-connector before entering the ICP torch. Integration time of *Nu Plasma II* was set to 0.3 s (equating to 133 cycles during the 40 s). Detailed instrumental operating settings and data calibrations were described in the study by Liu et al. (2008).

Standard zircons (including GJ-1, 91,500, Plešovice, Mud Tank, Penglai) were treated as quality control for every fifteen unknown samples. Zircon standard 91,500 yielded an average $^{176}Hf/^{177}Hf$ value of 0.282,313 ± 0.000010 (n = 14). Zircon standard GJ-1 yielded an average $^{176}Hf/^{177}Hf$ value of 0.282,013 ± 0.000009 (n = 26). Zircon standard Mud Tank yielded an average $^{176}Hf/^{177}Hf$ value of 0.282,520 ± 0.000008 (n = 13). Zircon standard Penglai yielded an average $^{176}Hf/^{177}Hf$ value of 0.282,907 ± 0.000008 (n = 14). Zircon standard Plešovice yielded an average $^{176}Hf/^{177}Hf$ value of 0.282,479 ± 0.000007 (n = 14). All the values of standards are accordant with previous works of Li et al. (2010), Sláma et al. (2008), and Yuan et al. (2008).

A ^{176}Lu decay constant of 1.865×10^{-11} year^{-1} and chondritic values of $^{176}Hf/^{177}Hf$ = 0.282,772 and $^{176}Lu/^{177}Hf$ = 0.0332 were adopted to calculate the initial $^{176}Hf/^{177}Hf$ ratios and ε_{Hf} (t) values (Blichert-Toft and Albarède, 1997). $T_{DM}C$ (zircon Hf isotope crustal model age) uses the average continental crustal $^{176}Lu/^{177}Hf$ ratio of 0.0113 and calculates following the study by Griffin et al. (2002).

Whole Rock Major and Trace Element

Major and trace elements of bulk-rock samples were analyzed at the Geochemistry Division of Australian Laboratory Services Chemex (Guangzhou) Co. Ltd. Major elements were analyzed by X-ray fluorescence spectrometry (PANalytical PW2424,

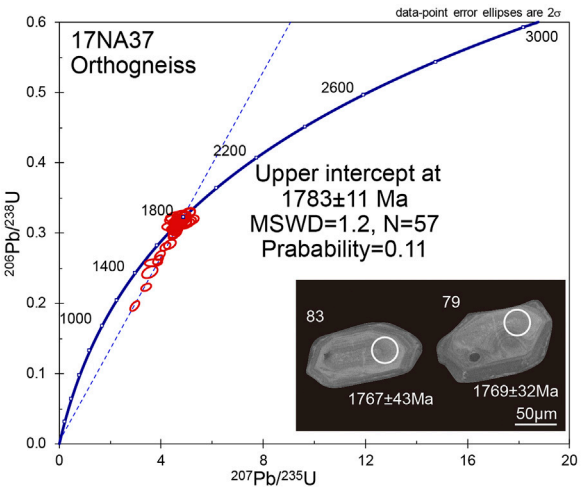

FIGURE 5 | Wetherill concordia diagram of orthogneiss sample 17NA37. The cathodoluminescent image of the representative zircons shows analyzed spots located in the core. The upper intercept age represents the assumed protolith crystallization age.

Netherlands). All samples were first milled to less than 200 mesh and then mixed with $Li_2B_4O_7$ to make homogeneous glass disks at 1,000°C for further analysis. The analytical precision of major elements was better than 1% (Liu et al., 2008).

The trace element concentration of the sample solutions was determined by inductively coupled plasma mass spectrometry (Agilent 7,900, America). About 50 mg of powder for every sample was added to a lithium metaborate flux, mixed well, and fused in a furnace at 1,025°C. The resulting melt was then cooled and dissolved in 100 ml of 4% HNO_3 solution for further analysis (Pearce, 2008). The analytical precision is better than 5% for most trace elements using the GSR-2 standard (Workman and Hart, 2005).

RESULTS

U-Pb Zircon Geochronology

Nine samples have been examined for zircon U-Pb geochronology along the Arun Valley in order to determine the age of these rock types forming individual thrust sheets (sample locations shown in **Figures 1**, **2**). Representative CL images show the location of analyzed spots that were targeted in the zircon cores to reveal the protolith age of metamorphic rocks. One orthogneiss sample was analyzed to constrain its crystallization age (**Figure 5**), and eight metasedimentary samples were analyzed to get their maximum sedimentary ages and to locate their provenance (**Figure 6**). Only those zircons with concordance ≥90% from metasedimentary rocks were used in this study (**Figure 6**).

MAIN CENTRAL THRUST ZONE

Eight samples from the MCTZ analyzed in this study can be divided into two different groups that are characterized by either single peak or multiple peaks (**Figure 7**). Sample 17NA03 of garnet-sillimanite schist from the uppermost part of the MCTZ is characterized by a major peak at around 1860 Ma and several Archean zircons (4%) (**Figure 7**). The maximum depositional age (MDA) of this sample generated at 1729 ± 39 Ma (3 grains, MSWD = 0.15). Among the analyzed zircons, 1.7–2.0 Ga grains are predominant (83%) and 2.4–2.6 Ga grains are sporadic (3%.) Paragneiss sample 17NA15 shows a prominent peak at 1860 Ma and MDA at 1787 ± 31 Ma (3 grains, MSWD = 0.27). In this sample, zircons ranging from 1.7 to 2.0 Ga make up 88% of the whole available zircons, and zircons of 2.4–2.6 Ga just account for 4% (**Figure 7**). Schist sample 17NA16 exhibited a more prominent peak at 1860 Ma with

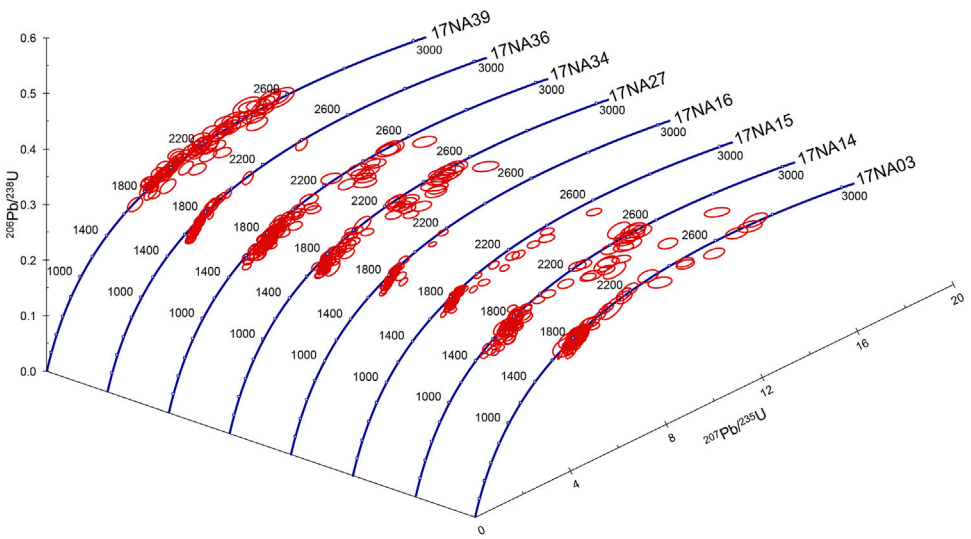

FIGURE 6 | Wetherill concordia diagram of detrital zircons. Detrital zircons with concordance >90% are used in this study. Error ellipses of data-point use 2 Sigma.

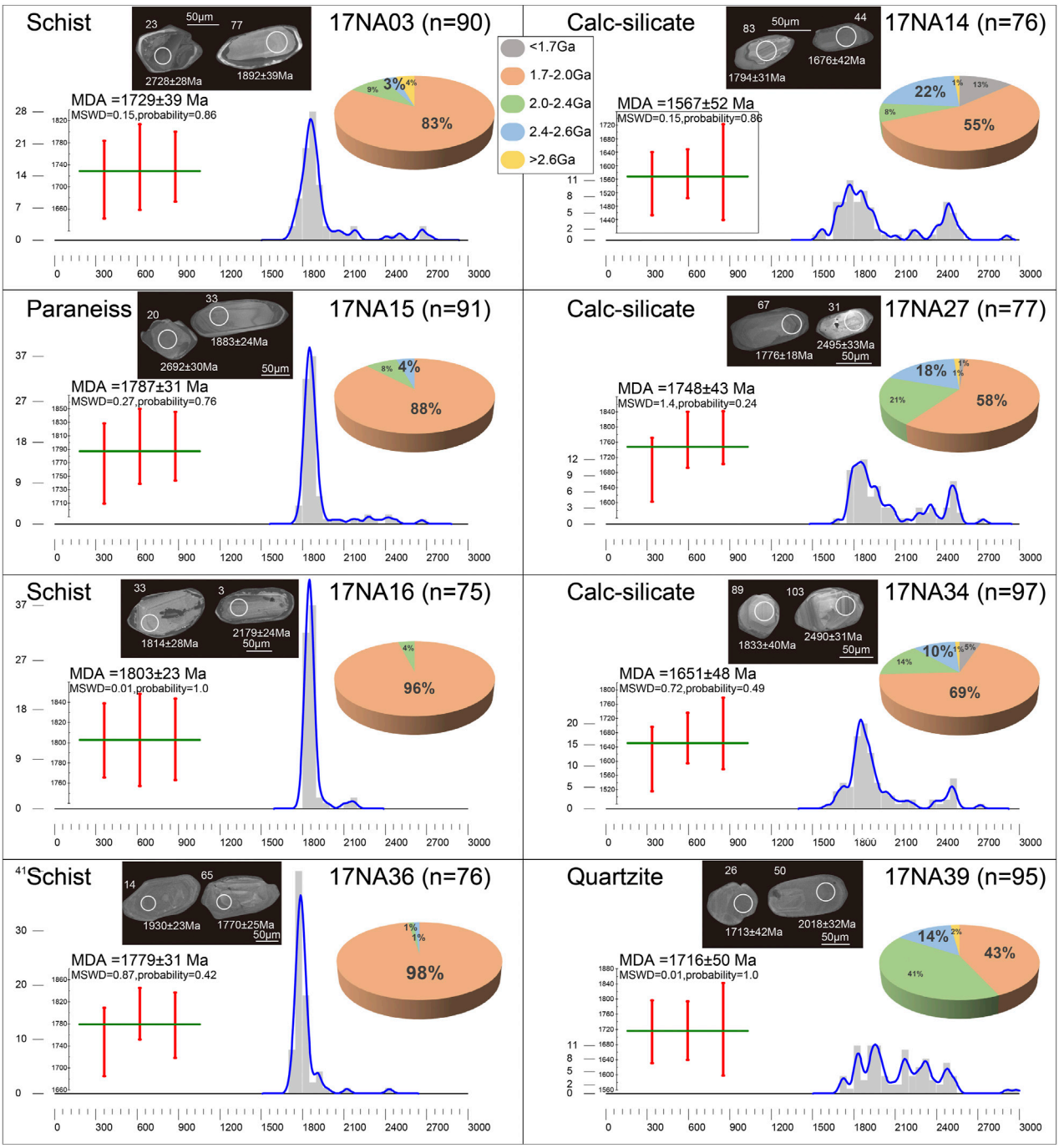

FIGURE 7 | Geochronological data for detrital zircons in metasedimentary rocks. The cathodoluminescent images of the representative zircons in each sample show analyzed spots located in the core. Pie charts show the percentage of the age of different age-groups. The maximum depositional age (MDA) is based on the mean weighted age of the three youngest zircons in each sample. Kernel density estimation diagrams are based on data of ^{207}Pb-^{206}Pb age with concordance higher than 90%. The left column shows the single peak of spectra, while the right column shows multiple peaks.

the MDA 1803 ± 23 Ma (3 grains, MSWD = 0.01), with only three zircons showing older ages (2.0–2.4 Ga) (**Figure 7**). Compared with the samples aforementioned, schist sample 17NA36 from the lower part of the MCTZ shows a similar unimodal spectrum but a slightly younger peak at 1800 Ma. This sample yielded MDA at 1779 ± 31 Ma (3 grains, MSWD = 0.87), with 98% zircons ranging in age from 1.7 to 2.0 Ga.

In the MCTZ, three calc-silicate samples from different sheets in the profile of the Arun Valley (17NA14, 17NA27, and 17NA34) have been dated and are characterized by

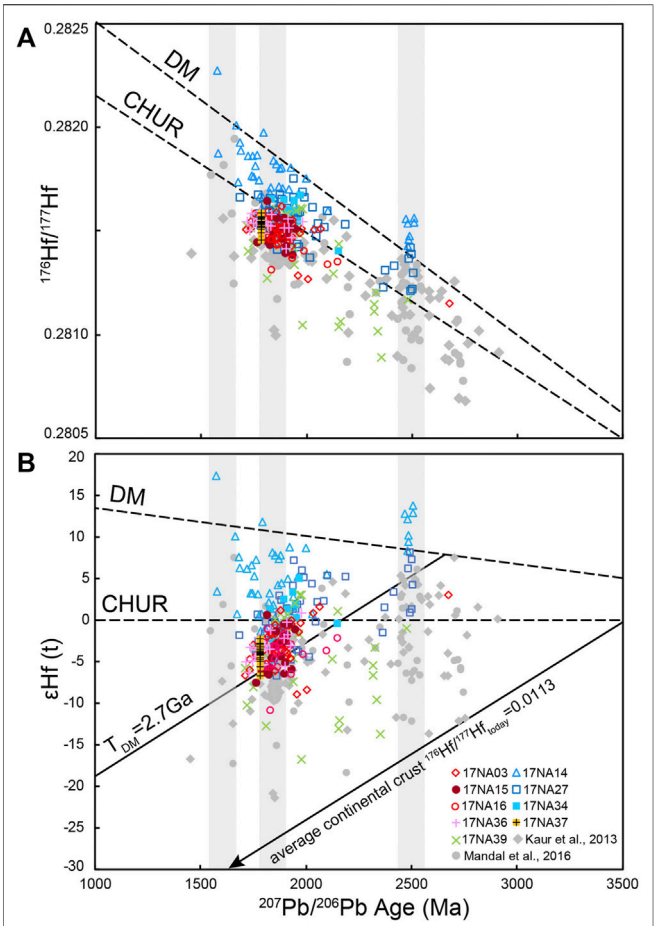

FIGURE 8 | (A) Plot of $^{176}Hf/^{177}Hf$ vs. $^{207}Pb/^{206}Pb$ ages of zircons for the orthogneiss and metasedimentary rocks in the Arun Valley. **(B)** Plot of ε_{Hf} (t) vs. $^{207}Pb/^{206}Pb$ ages of zircons. Reference data of Mandal et al. (2016) are from the Askot klippe, Kumaun of Northwest India, and data of Kaur et al. (2013) are from the Aravalli Supergroup of West India.

multiple peaks spanning the Paleoproterozoic era, with a prominent peak at 1860 Ma and a secondary peak at 2,500 Ma (**Figure 7**). Specifically, sample 17NA14 shows a younger MDA at 1,567 ± 52 Ma (3 grains, MSWD = 0.15). Zircons in this sample are dominated by 1.7–2.0 Ga (55%) and 2.4–2.6 Ga (22%) grains. Sample 17NA27 yielded an MDA at 1748 ± 43 Ma (3 grains, MSWD = 1.4). However, one youngest zircon was dated as ca. 1,680 Ma (**Figure 7**). In this sample, zircons of 1.7–2.0 Ga make up 58% and 2.4–2.6 Ga 18% of the whole zircon population. Sample 17NA34 yielded an MDA at 1,651 ± 48 Ma (3 grains, MSWD = 0.72), while 1.7–2.0 Ga zircons (69%) and 2.4–2.6 Ga zircons (10%) make up the dominant portion of the whole population (**Figure 7**).

An orthogneiss (17NA37) from the lower sheet of the MCTZ displays an upper intercept age of 1783 ± 11 Ma (MSWD = 1.2, 57 grains, **Figure 5**). Some discordant data and a poorly defined lower intercept are likely due to later metamorphism and subsequent Pb loss.

SETI FORMATION

The sample of quartzite (17NA39) from the lower Seti Formation lacks a dominant peak and is characterized by several peaks spanning the period of 1,650–2,550 Ma, with two isolated older data points at around 2,950 Ma. The measured zircons yielded MDA at 1716 ± 50 Ma (3 grains, MSWD = 0.01) (**Figure 7**). In this sample, zircons of 1.7–2.0 Ga and 2.0–2.4 Ga account for about 43 and 41%, respectively, of the entire zircon population (**Figure 7**).

Zircon Hf Isotope

Samples with a single peak and multiple peaks of the detrital zircon age spectrum showed different isotopic characteristics (**Figure 8**). On the one hand, the samples with a single age peak have relatively consistent $^{176}Hf/^{177}Hf$ (t) and ε_{Hf} (t) values and most of them are below the evolution line of Chondritic Uniform Reservoir (CHUR). On the other hand, the samples with multiple peak age spectrums have relative variable values, part of which $^{176}Hf/^{177}Hf$ (t) and ε_{Hf} (t) values of zircons are beyond the CHUR evolution line. The orthogneiss sample shows negative values of ε_{Hf} (t).

Detrital zircons from the schist and the paragneiss samples 17NA03, 17NA15, 17NA16, and 17NA36 with a single age peak yielded values of $^{176}Hf/^{177}Hf$ (t) ranging from 0.281,151 to 0.281,644 and ε_{Hf} (t) values ranging from −10.8 to 3.0 (**Figure 8**) (see **Supplementary Table S2** for detailed data on each of the zircons).

The zircons younger than 1.7–2.0 Ga from calc-silicate samples of 17NA14, 17NA27, and 17NA34 yielded values of $^{176}Hf/^{177}Hf$ (t) ranging from 0.281,405 to 0.282,009 and ε_{Hf} (t) values ranging from −4.7 to 8.8 (**Figure 8**). Zircons (2.4 Ga to 2.6 Ga) from 17NA14, 17NA27, and 17NA34 yielded values of $^{176}Hf/^{177}Hf$ (t) ranging from 0.281,207 to 0.281,564; the ε_{Hf} (t) values of these zircons ranged from 0.9 to 13.8 (**Figure 8**).

Zircons from quartzite sample 17NA39 younger than 2.0 Ga yielded values of $^{176}Hf/^{177}Hf$ (t) ranging from 0.281,047 to 0.281,622, and the ε_{Hf} (t) values of these zircons ranged from −16.8 to 3.0 (**Figure 8**). Zircons older than 2.0 Ga yielded values of $^{176}Hf/^{177}Hf$ (t) ranging from 0.280,890 to 0.281,438, and the ε_{Hf} (t) values of these zircons ranged from −13.7 to 1.0 (**Figure 8**).

Orthogneiss sample 17NA37 yielded zircons with $^{76}Hf/^{177}Hf$ (t) values ranging from 0.281,458 to 0.281,584, and the ε_{Hf} (t) values of these zircons ranged from −6.7 to −2.2 (**Figure 8**).

Whole-Rock Geochemistry

Orthogneiss sample 17NA37 is characterized by relatively high SiO_2 (69 wt.%) and K_2O (4 wt.%), high Al_2O_3 (14.7 wt.%), and medium Na_2O (2.3 wt.%) (**Figure 9A**). In the TAS plot, the sample shows subalkaline affinities and plots in the field of granodiorite (**Figure 9B**). The ASI index of this sample has a value of 1.3, showing a peraluminous characteristic (**Figure 9D**). Moreover, the discrimination diagram of 10,000*Ga/Al vs. Zr (Whalen et al., 1987; Wu et al., 2017) shows that the orthogneiss falls at the boundary between I, S,

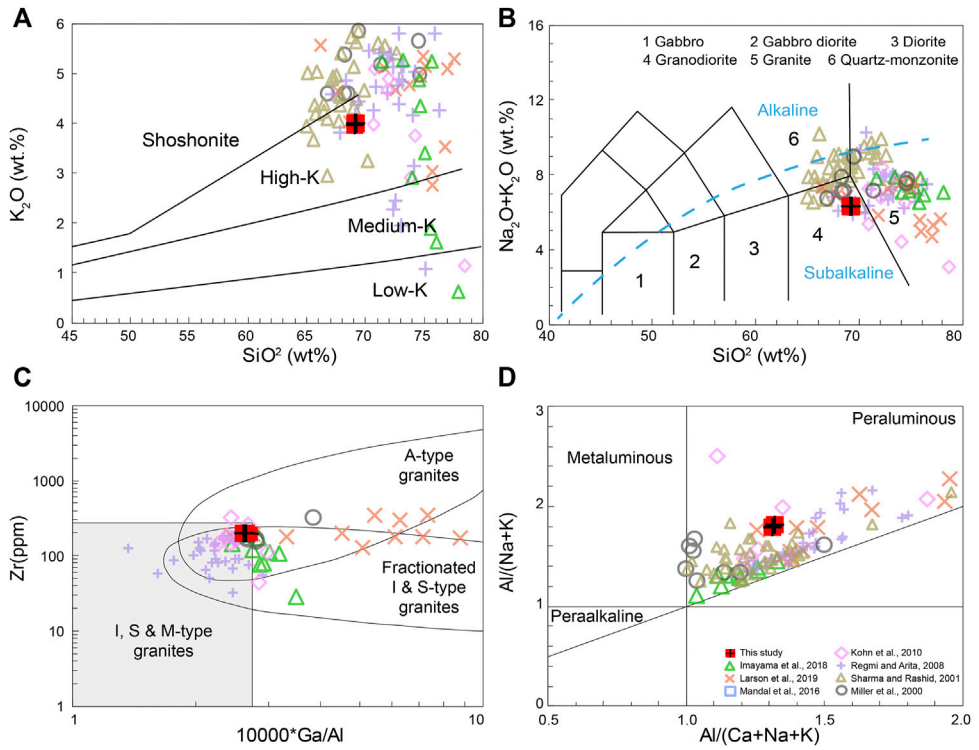

FIGURE 9 | Discrimination diagrams of granite. **(A)** K_2O vs. SiO_2 diagram (Irvine and Baragar, 1971); **(B)** TAS classification diagram (Middlemost, 1994); **(C)** diagram of 10000Ga/Al vs. Zr content (Whalen et al., 1987; Wu et al., 2017); **(D)** ANK vs. ACNK diagram (Maniar and Piccoli, 1989).

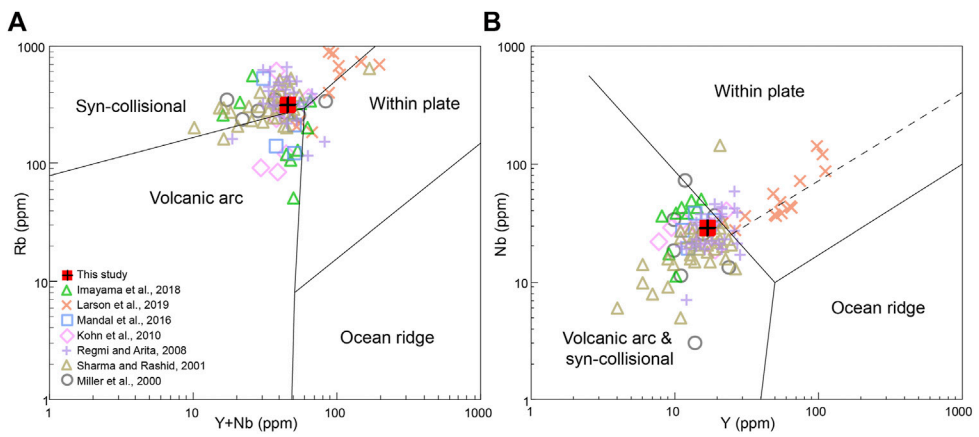

FIGURE 10 | Tectonic discrimination diagrams. **(A)** Y + Nb vs. Rb diagram and **(B)** Nb vs. Y diagram, after the study by Pearce et al. (1984) and Pearce (1996). The dashed line represents the upper compositional boundary of oceanic ridge granites from anomalous ridge segments. Data from Imayama et al. (2018), Larson et al. (2019), Mandal et al. (2016), Kohn et al. (2010), Regmi and Arita (2008), Sharma and Rashid (2001), Miller et al. (2000), and this study.

and M-type and A-type granites (**Figure 9C**). In the tectonic discrimination diagram of Rb vs. (Y + Nb) of Pearce (1996), our sample plots at the boundary between the "syn-collisional" and "volcanic arc" granitoid field (**Figure 10A**). Similarly, the orthogneiss plots at the "volcanic arc and syn-collisional" granitoid field in the Nb-Y diagram (**Figure 10B**).

The REE patterns of orthogneiss normalized by chondrite values are enriched in the LREE. Moreover, they exhibit a negative Eu anomaly (**Figure 11A**). Trace element abundance of the orthogneiss sample normalized to primitive mantle is shown in **Figure 11B**. They are characterized by high Th and U contents, and negative Sr anomalies.

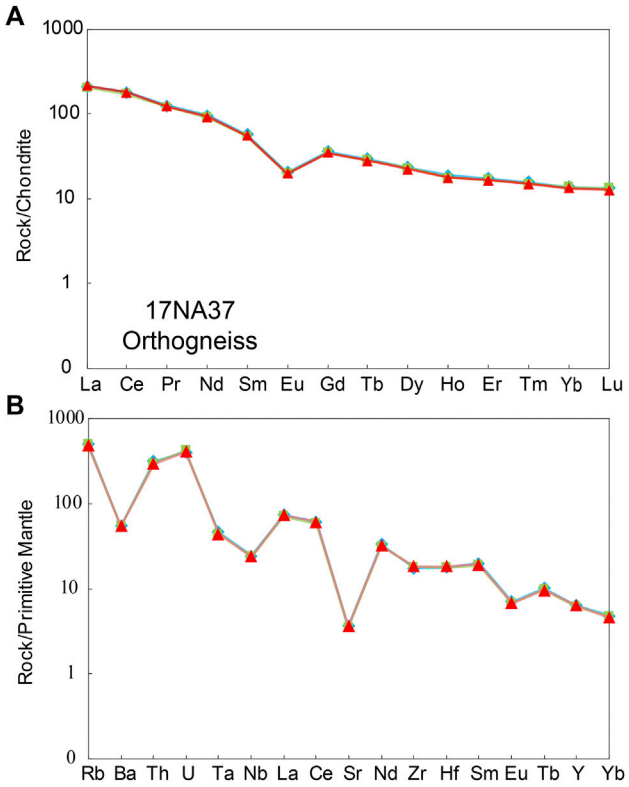

FIGURE 11 | (A) Chondrite-normalized rare Earth element (REE) patterns for orthogneiss. **(B)** Primitive mantle-normalized trace element variation diagrams. Normalization factors are from the study by Sun and McDonough (1989).

DISCUSSION

Origin and Relation of the Metasedimentary Rocks in the Lesser Himalaya Sequence

Previous studies distinguished several Paleoproterozoic strata like the Berinag, Kuncha, Fagfog, Kushma, and Seti Formations in the lower part of the LHS (Upreti et al., 1999; Martin et al., 2011). These formations are characterized by multiple peaks of the zircon age spectrum, that is, a primary peak at ca.1850 Ma and a secondary peak at 2,500 Ma (Martin et al., 2011; Mandal et al., 2016). These are also Paleoproterozoic strata characterized by a single peak of the zircon age spectrum such as the Munsiari Formation (Spencer et al., 2012). The studied metasedimentary rocks in the Arun Valley show marked differences in detrital zircons spectra and can be divided into two groups: the group of cal-silicate rocks and quartzite as well as the group of schists and paragneiss (**Figure 7**).

The calc-silicate rocks and quartzite samples with relatively younger MDA show multiple age spectra of detrital zircons. Those calc-silicate rocks, which have two major peaks at ca. 1850 Ma and 2,500 Ma, are similar to the zircon spectra of formations mentioned above (**Figure 7**). The older zircon age peak can be related to the Indian Craton which is characterized by ca. 2.5 Ga magmatism (Kohn et al., 2010). This implies that the northern Indian Craton acted as the main source for deposition of the protolith of the calc-silicate rocks. In particular, the quartzite sample of the Seti Formation in the lower part of the Arun Valley has an older MDA and more ~2.5 Ga zircons (**Figure 7**). This might indicate that it was deposited earlier and received more old sediments from the northern Indian Craton than the calc-silicate rocks. This kind of spectrum with greater proportions of older age from the basement reflects that it was deposited in a foreland basin, rifting basin, or back-arc basin (Cawood et al., 2012). However, considering VMS deposits found in the bottom of the LHS, the back-arc extensional setting with rifting basins is more reasonable in the northern Indian Craton (Mandal et al., 2016).

The schist and paragneiss with a single peak of the age spectrum indicate that these strata had abundant and unitary source. Their peak age of ca. 1850 Ma matches well with the Paleoproterozoic magmatism frequently reported from the northern Indian Craton. However, these rocks lack or contain very little amount of Archean zircons, which may imply that they have been deposited farther away from the northern Indian Craton. The single peak in the detrital zircon spectrum could also imply that the detrital zircons came from a single magmatic source and that the original sedimentary strata were deposited in a fore-arc basin (Cawood et al., 2012).

The Hf isotope of zircons also shows distinct differences between the calc-silicate rocks and the schists. All the zircons

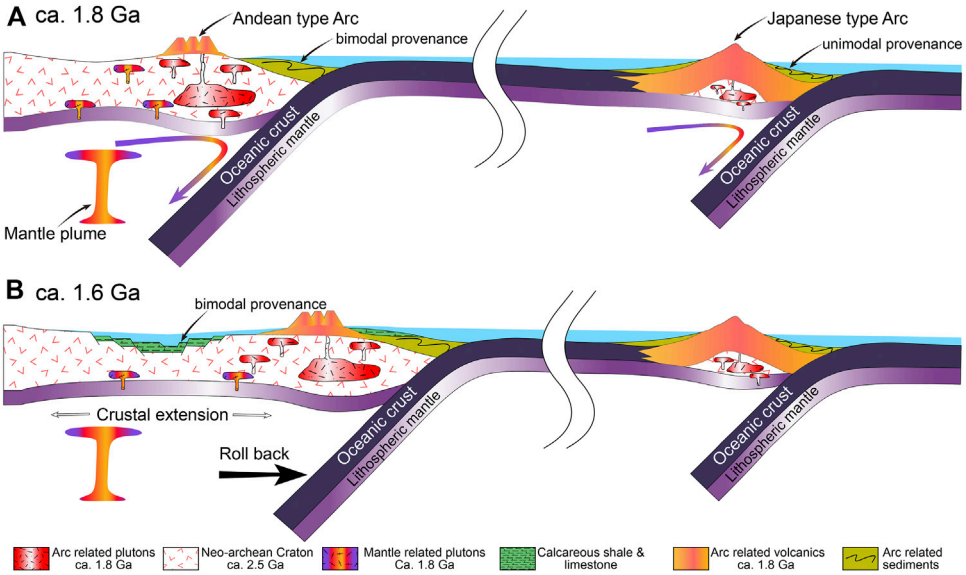

FIGURE 12 | Schematic diagrams of the Late Paleoproterozoic evolution of a two-arc system of the northern Indian Craton (left) and the newly defined Japan-type arc (right), modified from the study by Mandal et al. (2016). **(A)** At ca. 1.8 Ga there existed a two-arc system in the northern Indian Craton and its oceanic nearby domain. The Japanese-type arc contained limited Neoarchean crust material which melted as a magma chamber, which provided a unimodal source to the sediments. In contrast, the Andean-type arc provided a bimodal source for the sediments. **(B)** At ca.1.6 Ga, rollback of subduction slab and a mantle plume in the Andean-type arc resulted in back-arc rifting in the northern Indian Craton. The gap between the two arcs represents a remote location of the Japanese-type arc, far away from the Andean-type arc (see the text for detailed explanation).

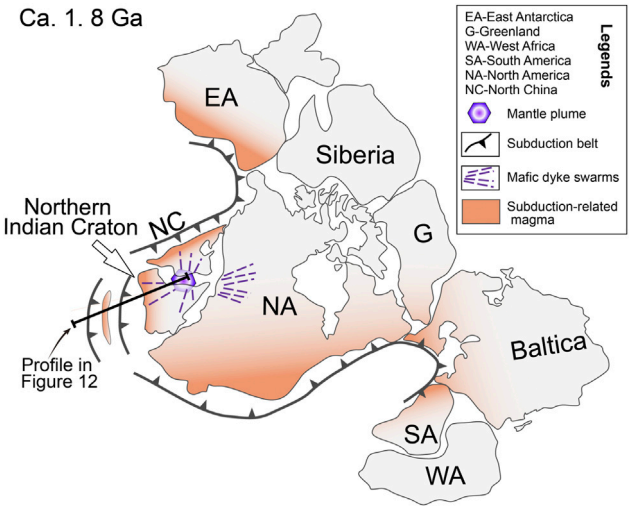

FIGURE 13 | An updated model for the ca. 1.8 Ga reconstruction of the supercontinent Columbia, modified from the study by Hou et al. (2008). In the modified model, there existed a two-arc system with double subduction zones in the northern margin of the northern Indian Craton, and the approximate position of the profiles in **Figure 12** is shown.

from schist samples with a single peak age spectrum show negative values of ε_{Hf} (t), suggesting that the continental crust played a pivotal role in their formation (**Figure 8B**). In addition, Hf model ages around ca. 2,500 Ma of these zircons indicate remobilization of Archean crust. Altogether, zircon U-Pb and ε_{Hf} (t) data may suggest that the protoliths of the schists are derived from a unitary source in a fore-arc basin of an arc that has a continental basement. The zircons with the ca. 1850 Ma peak from calc-silicate rock samples show both positive and negative ε_{Hf} (t) values (**Figure 8B**), which is in accordance with data published in previous studies (Kaur et al., 2013; Mandal et al., 2016). The orthogneiss in the LHS show generally negative ε_{Hf} (t) values, and so far, igneous rocks with zircons of positive values have not been reported (Mandal et al., 2016). Therefore, there should be other sources of Paleoproterozoic igneous rocks that provided the zircons with positive ε_{Hf} (t) such as arc-related mafic rocks and mantle plume magmas in the northern Indian craton which have been proposed by some authors (Hou et al., 2008; Kohn et al., 2010).

The difference in the Hf isotopes from zircons between two groups of metasedimentary rocks implies that they might have been deposited in two isolated arcs. The calc-silicate rocks with positive ε_{Hf} (t) zircons indicate that they might have been deposited in the back-arc extensional basin in the northern Indian Craton. However, the lack of zircons with positive ε_{Hf} (t) in the group of schists indicates that they might have been deposited in an arc isolated from the northern Indian Craton, and the isolated arc might build in a microcontinent. This kind of arc is similar to the Japanese arc which contains older basement drifting from the eastern Eurasian plate (Taira, 2001; Xiao et al., 2010). The multiple age spectra of the calc-silicate rocks and quartzite may indicate the deposition of protolith sediments in the back-arc basin of a continental arc like the Andean arc built in the South American Craton (Cawood et al., 2012).

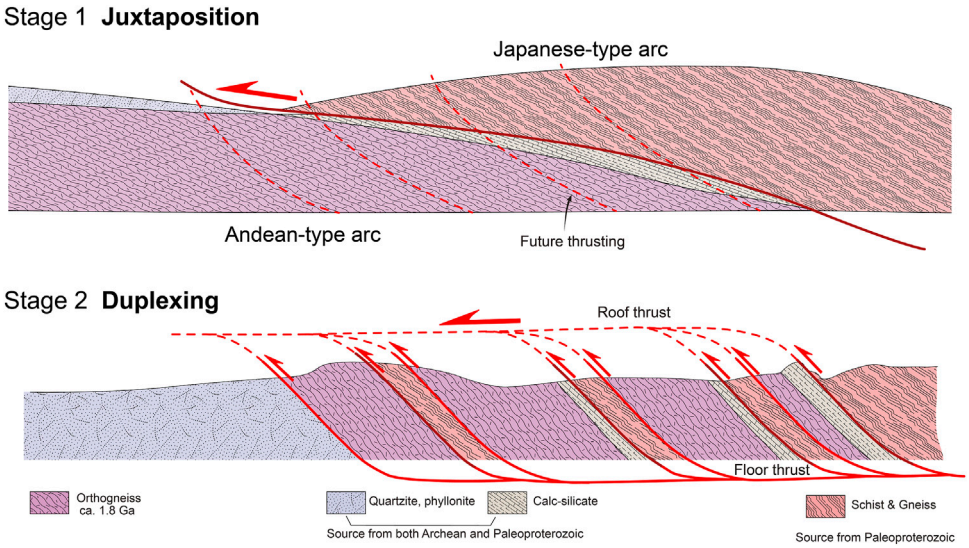

FIGURE 14 | Schematic diagrams of the structural and tectonic evolution of the two-arc system along the northern Indian Craton. At stage 1 of juxtaposition, the margin of the Japanese-type arc with unimodal source thrusted over the margin of the Andean-type arc with bimodal source. At stage 2 of duplexing, the out-of-sequence thrust system formed the modern structure of the Arun Valley.

Paleoproterozoic Magmatism in Northern Indian Craton

Geochemical data of the orthogneiss in this study indicate affinity to the syn-collisional or arc magmatism close to the within plate magmatic field (**Figure 10**). Taking into account all the reported Paleoproterozoic orthogneisses, the granitoid rocks in the LHS show various compositions (Ahmad et al., 1999; Miller et al., 2000; Sharma and Rashid, 2001; Regmi and Arita, 2008; Kohn et al., 2010; Sakai et al., 2013; Mandal et al., 2016; Imayama et al., 2018; Larson et al., 2019). The high Sr isotopic ratios and S-type nature of these granitoid rocks indicate a crustal melting source and intracontinental rifting setting (Imayama et al., 2018; Larson et al., 2019). However, the existence of a continental arc associated with a back-arc extension cannot be excluded (Kohn et al., 2010; Mandal et al., 2016). Sakai et al. (2013) pointed out that the lack of accretionary complex could exclude the continental arc background. However, a group of marble, calc-silicate in this study, and MORB-type meta-mafic rocks reported in this area might represent slices of a Paleoproterozoic accretionary complex (Corrie et al., 2010; Wang et al., 2017). Orthogneiss sample 17NA37 in this study with negative Nb and Sr anomalies and high Th, U, Ce, and Rb anomalies also suggests that the protolith of orthogneiss has been influenced by the continental arc (**Figure 11**) (Mandal et al., 2016).

Considering the intensive convergence of the Himalayas in the Cenozoic, the arc-related rocks can be deeply buried and reworked in the GHS (DeCelles, 2001). This can be supported by the presence of metasedimentary rocks with the volcanogenic source that are commonly exposed at the boundary zone between the GHS and LHS (Kohn et al., 2010). Therefore, the wild compositional range of orthogneisses in the LHS cannot be explained by a single petro-genetic tectonic model of continental rifting. Instead, the continental arc and related back-arc rifting can explain a diversity of 1.8 Ga felsic and mafic rocks in the region (Kohn et al., 2010).

Paleoproterozoic Tectonic Model and Implications for Columbia Supercontinent

Based on the data of this study, a model of two arc systems, that is, a Japanese-type arc and an Andean type arc, is proposed to co-exist along the active margin of the Columbia supercontinent, which formed the LHS of the Cenozoic Himalayan orogenic belt. The Japanese-type arc was firmly established on the Archean crust. However, the Archean crust did not provide any material to the arc-relevant basins. It might just serve as a basement and melted into a magma chamber, thereby providing the unimodal arc source to sediments at 1.8 Ga (**Figure 12A**).

On the other hand, the Andean-type arc may have developed at the continental margin of the northern Indian craton (**Figure 12A**). Continuous subduction could result in extension in the back-arc domain and related crustal melting. In this region, a large variety of magma with distinct Hf isotopic signature in the lower-middle crust could develop while marble and calcareous shales could be deposited at ca. 1.6 Ga (**Figure 12A**). All of these sediments have bimodal zircon sources from the Paleoproterozoic igneous rocks and Neoarchean sources of the northern Indian Craton.

Thus, our data shed new light on the reconstruction of the Columbia supercontinent with an active margin along the northern Indian Craton (**Figure 13**) (Hou et al., 2008; Kohn

et al., 2010). In our new model, a two-arc system is proposed to co-exist along the active margin of the Columbia supercontinent.

Tectonic Juxtaposition and Duplex Structure of Eastern Himalaya

The duplication of schists and calc-silicate rocks revealed a complicated duplex structure in the MCT zone, and before the duplexing, the two arcs should have been juxtaposed with each other (**Figures 2**, **14**). In this region, a sequence of thrusts has been revealed by previous studies, but only the Cenozoic metamorphism has been reported and linked to these deformations (Groppo et al., 2009; Ambrose et al., 2015; Larson et al., 2015). There is absence of metamorphic events reported before the Cenozoic in the LHS and MCTZ, which means the time for the juxtaposition of two arcs is obscure (DeCelles et al., 2000; Kohn et al., 2010; Martin, 2017). Two scenarios can be imagined: 1) first, the Japanese-type arc had accreted onto the northern Indian Craton in the Precambrian time. In this case, the information of accretion such as metamorphic events and magmatic events may have been cryptic, that is, buried beneath the GHS or covered by high-ultrahigh temperature metamorphism during the intensive Cenozoic convergence (Wang et al., 2021). 2) The second possibility is that the Japanese-type arc did not accrete onto the northern Indian Craton until the Cenozoic time. In this case, the Japanese-type independent arc was isolated from the northern Indian Craton. It might accrete to some other cratons like Yilgarn Craton along the active margin of the supercontinent of Columbia. The rifting of supercontinent Gondwana in Cretaceous time might drift the Japanese-type arc northward, and the later Himalayan orogeny makes the two Paleoproterozoic arcs juxtaposed and imbricated with each other in the Cenozoic era (Xiao et al., 2017; Li et al., 2021). In particular, this occasion requires the last collision between the Indian plate and Eurasian plate to be along the MCT in the Himalayan orogeny (van Hinsbergen et al., 2012; Xiao et al., 2017).

In either cases above, the juxtaposition and following duplexing of two groups of schists and calc-silicate rocks led to the formation of the MCTZ (**Figure 14**) (Larson et al., 2015). In the first stage, the Japanese-type arc with protolith of schists was juxtaposed and thrusted over the Andean-type arc with protolith of calc-silicate rocks. In the second stage, continuous convergence forced the Japanese-type arc imbricated with the Andean-type arc to form the structure of the duplex.

Combined with the structural relationship and the detailed analysis of the protoliths of the LHS and MCTZ, our study shed light on the structure of the Himalayan orogenic belt that these crustal-scale thrusts between different units may have been inherited from previous tectonic boundaries.

CONCLUSION

Based on our field mapping, together with our new data on whole rock geochemistry, zircon U-Pb age, and Hf isotopes, two groups of metasedimentary rocks are distinguished. The first group is represented by schists and paragneiss with a single Paleoproterozoic age peak and negative zircon ε_{Hf} (t) values. These data are interpreted as a deposition of sediments in the proximity of an immature Japanese-type arc spatially isolated from the northern Indian Craton. The second rock group is represented by calc-silicate rocks and quartzite with a multiple age peaks spectrum with the youngest Paleoproterozoic peak. Their zircon ε_{Hf} (t) values and characteristics of associated orthogneiss may indicate their deposition in the back-arc or fore-arc basins of an Andean-type arc developed on the northern margin of the northern Indian Craton. We suggested that a two-arc system developed at the northern Indian Craton during Paleoproterozoic time, and the two arcs were juxtaposed either in Paleoproterozoic or Cenozoic time and finally imbricated during the Cenozoic duplexing.

DATA AVAILABILITY STATEMENT

The original contributions presented in the study are included in the article/**Supplementary Material**, further inquiries can be directed to the corresponding author.

AUTHOR CONTRIBUTIONS

All authors listed have made a substantial, direct, and intellectual contribution to the work and approved it for publication.

FUNDING

This study was funded by the National Natural Science Foundation of China (41888101), the Science and Technology Major Project of Xinjiang Uygur Autonomous Region, China (2021A03001), the National Key R&D Program of China (2017YFC0601206), and the Key Research Program of Frontier Sciences, CAS (QYZDJ-SSW-SYS012). This is a contribution to IGCP 662.

ACKNOWLEDGMENTS

We thank Steve Collet, Ji'en Zhang, Zhiyong Zhang, and Zhen Yan for the discussion on the tectonics of the Himalayan orogen. The constructive comments and suggestions from the editors and two formal reviewers are greatly acknowledged.

SUPPLEMENTARY MATERIAL

The Supplementary Material for this article can be found online at: https://www.frontiersin.org/articles/10.3389/feart.2022.890171/full#supplementary-material

REFERENCES

Ahmad, T., Mukherjee, P., and Trivedi, J. (1999). Geochemistry of Precambrian Mafic Magmatic Rocks of the Western Himalaya, India: Petrogenetic and Tectonic Implications. *Chem. Geology.* 160 (1-2), 103–119. doi:10.1016/s0009-2541(99)00063-7

Ambrose, T. K., Larson, K. P., Guilmette, C., Cottle, J. M., Buckingham, H., and Rai, S. (2015). Lateral Extrusion, Underplating, and Out-Of-Sequence Thrusting within the Himalayan Metamorphic Core, Kanchenjunga, Nepal. *Lithosphere* 7 (4), 441–464. doi:10.1130/l437.1

Blichert-Toft, J., and Albarède, F. (1997). The Lu-Hf Isotope Geochemistry of Chondrites and the Evolution of the Mantle-Crust System. *Earth Planet. Sci. Lett.* 148 (1), 243–258. doi:10.1016/S0012-821X(97)00040-X

Cawood, P. A., Hawkesworth, C. J., and Dhuime, B. (2012). Detrital Zircon Record and Tectonic Setting. *Geology* 40 (10), 875–878. doi:10.1130/g32945.1

Corrie, S. L., Kohn, M. J., and Vervoort, J. D. (2010). Young Eclogite from the Greater Himalayan Sequence, Arun Valley, Eastern Nepal: P-T-T Path and Tectonic Implications. *Earth Planet. Sci. Lett.* 289 (3-4), 406–416. doi:10.1016/j.epsl.2009.11.029

DeCelles, P. G., Gehrels, G. E., Quade, J., LaReau, B., and Spurlin, M. (2000). Tectonic Implications of U-Pb Zircon Ages of the Himalayan Orogenic belt in Nepal. *Science* 288 (5465), 497–499. doi:10.1126/science.288.5465.497

DeCelles, P. G., Robinson, D. M., Quade, J., Ojha, T. P., Garzione, C. N., Copeland, P., et al. (2001). Stratigraphy, Structure, and Tectonic Evolution of the Himalayan Fold-Thrust belt in Western Nepal. *Tectonics* 20, 487–509. doi:10.1029/2000TC001226

Gansser, A. (1964). *Geology of the Himalayas*. New York, NY: Wiley InterScience 289.

Goscombe, B., Gray, D., and Foster, D. A. (2018). Metamorphic Response to Collision in the Central Himalayan Orogen. *Gondwana Res.* 57, 191–265. doi:10.1016/j.gr.2018.02.002

Goscombe, B., Gray, D., and Hand, M. (2006). Crustal Architecture of the Himalayan Metamorphic Front in Eastern Nepal. *Gondwana Res.* 10 (3-4), 232–255. doi:10.1016/j.gr.2006.05.003

Griffin, W. L., Wang, X., Jackson, S. E., Pearson, N. J., O'Reilly, S. Y., Xu, X., et al. (2002). Zircon Chemistry and Magma Mixing, SE China: *In-Situ* Analysis of Hf Isotopes, Tonglu and Pingtan Igneous Complexes. *Lithos* 61 (3), 237–269. doi:10.1016/S0024-4937(02)00082-8

Groppo, C., Lombardo, B., Rolfo, F., and Pertusati, P. (2007). Clockwise Exhumation Path of Granulitized Eclogites from the Ama Drime Range (Eastern Himalayas). *J. Metamorph Geol.* 25 (1), 51–75. doi:10.1111/j.1525-1314.2006.00678.x

Groppo, C., Rolfo, F., and Lombardo, B. (2009). P-T Evolution across the Main Central Thrust Zone (Eastern Nepal): Hidden Discontinuities Revealed by Petrology. *J. Pet.* 50 (6), 1149–1180. doi:10.1093/petrology/egp036

Hou, G., Santosh, M., Qian, X., Lister, G. S., and Li, J. (2008). Configuration of the Late Paleoproterozoic Supercontinent Columbia: Insights from Radiating Mafic Dyke Swarms. *Gondwana Res.* 14 (3), 395–409. doi:10.1016/j.gr.2008.01.010

Imayama, T., Arita, K., Fukuyama, M., Yi, K., and Kawabata, R. (2018). 1.74 Ga Crustal Melting after Rifting at the Northern Indian Margin: Investigation of Mylonitic Orthogneisses in the Kathmandu Area, central Nepal. *Int. Geology. Rev.* 61 (10), 1207–1221. doi:10.1080/00206814.2018.1504329

Irvine, T. N., and Baragar, W. R. A. (1971). A Guide to the Chemical Classification of the Common Volcanic Rocks. *Can. J. Earth Sci.* 8 (5), 523–548. doi:10.1139/e71-055

Jackson, S. E., Pearson, N. J., Griffin, W. L., and Belousova, E. A. (2004). The Application of Laser Ablation-Inductively Coupled Plasma-Mass Spectrometry to *In Situ* U-Pb Zircon Geochronology. *Chem. Geology.* 211 (1), 47–69. doi:10.1016/j.chemgeo.2004.06.017

Kali, E., Leloup, P. H., Arnaud, N., Mahéo, G., Liu, D., Boutonnet, E., et al. (2010). Exhumation History of the Deepest central Himalayan Rocks, Ama Drime Range: Key Pressure-Temperature-Deformation-Time Constraints on Orogenic Models. *Tectonics* 29, a–n. doi:10.1029/2009tc002551

Kaur, P., Zeh, A., Chaudhri, N., Gerdes, A., and Okrusch, M. (2013). Nature of Magmatism and Sedimentation at a Columbia Active Margin: Insights from Combined U-Pb and Lu-Hf Isotope Data of Detrital Zircons from NW India. *Gondwana Res.* 23 (3), 1040–1052. doi:10.1016/j.gr.2012.07.008

Kohn, M. J., Paul, S. K., and Corrie, S. L. (2010). The Lower Lesser Himalayan Sequence: A Paleoproterozoic Arc on the Northern Margin of the Indian Plate. *Geol. Soc. America Bull.* 122 (3-4), 323–335. doi:10.1130/B26587.1

Larson, K. P., Ambrose, T. K., Webb, A. A. G., Cottle, J. M., and Shrestha, S. (2015). Reconciling Himalayan Midcrustal Discontinuities: The Main Central Thrust System. *Earth Planet. Sci. Lett.* 429, 139–146. doi:10.1016/j.epsl.2015.07.070

Larson, K. P., Godin, L., Davis, W. J., and Davis, D. W. (2010). Out-of-sequence Deformation and Expansion of the Himalayan Orogenic Wedge: Insight from the Changgo Culmination, South central Tibet. *Tectonics* 29, a–n. doi:10.1029/2008tc002393

Larson, K., Piercey, S., and Cottle, J. (2019). Preservation of a Paleoproterozoic Rifted Margin in the Himalaya: Insight from the Ulleri-Phaplu-Melung Orthogneiss. *Geosci. Front.* 10 (3), 873–883. doi:10.1016/j.gsf.2017.05.010

Le Fort, P. (1975). Himalayas: the Collided Range. Present Knowledge of the continental Arc. *Am. J. Sci.* 275 (1), 1–44.

Li, R., Ao, S., Xiao, W., Windley, B. F., Zhan, M., Huang, P., et al. (2021). Tectonic Setting and Provenance of Early Cretaceous Strata in the Footwall of Main Central Thrust, Eastern Nepal: Implications for the Archipelago Palaeogeography of the Neo-Tethys. *Geol. J.* 56 (4), 1958–1973. doi:10.1002/gj.4035

Li, X.-H., Long, W.-G., Li, Q.-L., Liu, Y., Zheng, Y.-F., Yang, Y.-H., et al. (2010). Penglai Zircon Megacrysts: A Potential New Working Reference Material for Microbeam Determination of Hf-O Isotopes and U-Pb Age. *Geostandards Geoanalytical Res.* 34 (2), 117–134. doi:10.1111/j.1751-908X.2010.00036.x

Liu, Y., Hu, Z., Gao, S., Günther, D., Xu, J., Gao, C., et al. (2008). *In Situ* analysis of Major and Trace Elements of Anhydrous Minerals by LA-ICP-MS without Applying an Internal Standard. *Chem. Geology.* 257 (1-2), 34–43. doi:10.1016/j.chemgeo.2008.08.004

Lombardo, B., Pertusati, P., and Borghi, S. (1993). Geology and Tectonomagmatic Evolution of the Eastern Himalaya along the Chomolungma-Makalu Transect. *Geol. Soc. Lond. Spec. Publications* 74 (1), 341–355. doi:10.1144/gsl.sp.1993.074.01.23

Ludwig, K. (2008). *Isoplot Version 4.15: A Geochronological Toolkit for Microsoft Excel*. Berkeley Geochronology Center, Special Publication, 247–270.

Mandal, S., Robinson, D. M., Kohn, M. J., Khanal, S., Das, O., and Bose, S. (2016). Zircon U-Pb Ages and Hf Isotopes of the Askot Klippe, Kumaun, Northwest India: Implications for Paleoproterozoic Tectonics, basin Evolution and Associated Metallogeny of the Northern Indian Cratonic Margin. *Tectonics* 35 (4), 965–982. doi:10.1002/2015TC004064

Maniar, P. D., and Piccoli, P. M. (1989). Tectonic Discrimination of Granitoids. *GSA Bull.* 101 (5), 635–643. doi:10.1130/0016-7606(1989)10110.1130/0016-7606(1989)101<0635:tdog>2.3.co;2

Martin, A. J. (2017). A Review of Himalayan Stratigraphy, Magmatism, and Structure. *Gondwana Res.* 49, 42–80. doi:10.1016/j.gr.2017.04.031

Martin, A. J., Burgy, K. D., Kaufman, A. J., and Gehrels, G. E. (2011). Stratigraphic and Tectonic Implications of Field and Isotopic Constraints on Depositional Ages of Proterozoic Lesser Himalayan Rocks in central Nepal. *Precambrian Res.* 185 (1-2), 1–17. doi:10.1016/j.precamres.2010.11.003

Meier, K., and Hiltner, E. (1993). Deformation and Metamorphism within the Main Central Thrust Zone, Arun Tectonic Window, Eastern Nepal. *Geol. Soc. Lond. Spec. Publications* 74 (1), 511–523. doi:10.1144/gsl.sp.1993.074.01.34

Middlemost, E. A. K. (1994). Naming Materials in the Magma/igneous Rock System. *Earth-Science Rev.* 37 (3), 215–224. doi:10.1016/0012-8252(94)90029-9

Miller, C., Klötzli, U., Frank, W., Thöni, M., and Grasemann, B. (2000). Proterozoic Crustal Evolution in the NW Himalaya (India) as Recorded by Circa 1.80 Ga Mafic and 1.84 Ga Granitic Magmatism. *Precambrian Res.* 103 (3), 191–206. doi:10.1016/S0301-9268(00)00091-7

Pearce, J. A. (2008). Geochemical Fingerprinting of Oceanic Basalts with Applications to Ophiolite Classification and the Search for Archean Oceanic Crust. *Lithos* 100 (1), 14–48. doi:10.1016/j.lithos.2007.06.016

Pearce, J. A., Harris, N. B. W., and Tindle, A. G. (1984). Trace Element Discrimination Diagrams for the Tectonic Interpretation of Granitic Rocks. *J. Pet.* 25 (4), 956–983. doi:10.1093/petrology/25.4.956

Pearce, J. (1996). Sources and Settings of Granitic Rocks. *Episodes* 19, 120–125. doi:10.18814/epiiugs/1996/v19i4/005

Regmi, K. R., and Arita, K. (2008). Major and Trace Element Geochemistry of Augen Gneisses from the Higher Himalayan Crystalline Zone, Main Central

Thrust Zone and Lesser Himalayan Dome in Tamakoshi-Likhu Khola Area, East Nepal. *Himalayan Geology.* 29 (2), 95–108.

Robinson, D. M., DeCelles, P. G., Patchett, P. J., and Garzione, C. N. (2001). The Kinematic Evolution of the Nepalese Himalaya Interpreted from Nd Isotopes. *Earth Planet. Sci. Lett.* 192 (4), 507–521. doi:10.1016/S0012-821x(01)00451-4

Sakai, H., Iwano, H., Danhara, T., Takigami, Y., Rai, S. M., Upreti, B. N., et al. (2013). Rift-related Origin of the Paleoproterozoic Kuncha Formation, and Cooling History of the Kuncha Nappe and Taplejung Granites, Eastern Nepal Lesser Himalaya: a Multichronological Approach. *Isl. Arc* 22 (3), 338–360. doi:10.1111/iar.12021

Schelling, D. (1992). The Tectonostratigraphy and Structure of the Eastern Nepal Himalaya. *Tectonics* 11 (5), 925–943. doi:10.1029/92tc00213

Sharma, K. K., and Rashid, S. A. (2001). Geochemical Evolution of Peraluminous Paleoproterozoic Bandal Orthogneiss NW, Himalaya, Himachal Pradesh, India: Implications for the Ancient Crustal Growth in the Himalaya. *J. Asian Earth Sci.* 19 (4), 413–428. doi:10.1016/S1367-9120(00)00052-3

Shrestha, S., Shrestha, J., and Sharma, S. (1984). *Geological Map of Eastern Nepal, 1: 250 000.* Kathmandu: Ministry of Industry, Department of Mines and Geology, Lainchour.

Sláma, J., Košler, J., Condon, D. J., Crowley, J. L., Gerdes, A., Hanchar, J. M., et al. (2008). Plešovice Zircon - A New Natural Reference Material for U-Pb and Hf Isotopic Microanalysis. *Chem. Geology.* 249 (1), 1–35. doi:10.1016/j.chemgeo.2007.11.005

Spencer, C. J., Harris, R. A., and Dorais, M. J. (2012). Depositional Provenance of the Himalayan Metamorphic Core of Garhwal Region, India: Constrained by U-Pb and Hf Isotopes in Zircons. *Gondwana Res.* 22 (1), 26–35. doi:10.1016/j.gr.2011.10.004

Sun, S.-s., and McDonough, W. F. (1989). Chemical and Isotopic Systematics of Oceanic Basalts: Implications for Mantle Composition and Processes. *Geol. Soc. Lond. Spec. Publications* 42 (1), 313–345. doi:10.1144/gsl.sp.1989.042.01.19

Taira, A. (2001). Tectonic Evolution of the Japanese Island Arc System. *Annu. Rev. Earth Planet. Sci.* 29, 109–134. doi:10.1146/annurev.earth.29.1.109

Upreti, B. N., Le Fort, P., Macfarlane, A., Sorkhabi, R. B., and Quade, J. (1999). Lesser Himalayan Crystalline Nappes of Nepal: Problems of Their Origin. *Geol. Soc. America* v328. doi:10.1130/0-8137-2328-0.225

van Hinsbergen, D. J. J., Lippert, P. C., Dupont-Nivet, G., McQuarrie, N., Doubrovine, P. V., Spakman, W., et al. (2012). Greater India Basin Hypothesis and a Two-Stage Cenozoic Collision between India and Asia. *Proc. Natl. Acad. Sci. U.S.A.* 109, 7659–7664. doi:10.1073/pnas.1117262109

Vermeesch, P. (2012). On the Visualisation of Detrital Age Distributions. *Chem. Geology.* 312-313, 190–194. doi:10.1016/j.chemgeo.2012.04.021

Wang, J.-M., Lanari, P., Wu, F.-Y., Zhang, J.-J., Khanal, G. P., and Yang, L. (2021). First Evidence of Eclogites Overprinted by Ultrahigh Temperature Metamorphism in Everest East, Himalaya: Implications for Collisional Tectonics on Early Earth. *Earth Planet. Sci. Lett.* 558, 116760. doi:10.1016/j.epsl.2021.116760

Wang, Y., Zhang, L., Zhang, J., and Wei, C. (2017). The Youngest Eclogite in central Himalaya: P-T Path, U-Pb Zircon Age and its Tectonic Implication. *Gondwana Res.* 41, 188–206. doi:10.1016/j.gr.2015.10.013

Whalen, J. B., Currie, K. L., and Chappell, B. W. (1987). A-type Granites: Geochemical Characteristics, Discrimination and Petrogenesis. *Contrib. Mineral. Petrol.* 95 (4), 407–419. doi:10.1007/BF00402202

Whitney, D. L., and Evans, B. W. (2010). Abbreviations for Names of Rock-Forming Minerals. *Am. Mineral.* 95 (1), 185–187. doi:10.2138/am.2010.3371

Wiedenbeck, M., Allé, P., Corfu, F., Griffin, W. L., Meier, M., Oberli, F., et al. (1995). Three Natural Zircon Standards for U-Th-Pb, Lu-Hf, Trace Element and REE Analyses. *Geostandards Newsl.* 19 (1), 1–23. doi:10.1111/j.1751-908X.1995.tb00147.x

Workman, R. K., and Hart, S. R. (2005). Major and Trace Element Composition of the Depleted MORB Mantle (DMM). *Earth Planet. Sci. Lett.* 231 (1), 53–72. doi:10.1016/j.epsl.2004.12.005

Wu, F., Liu, X., Ji, W., Wang, J., and Yang, L. (2017). Highly Fractionated Granites: Recognition and Research. *Sci. China Earth Sci.* 60 (7), 1201–1219. doi:10.1007/s11430-016-5139-1

Xiao, W., Ao, S., Yang, L., Han, C., Wan, B., Zhang, J. E., et al. (2017). Anatomy of Composition and Nature of Plate Convergence: Insights for Alternative Thoughts for Terminal India-Eurasia Collision. *Sci. China Earth Sci.* 60 (6), 1015–1039. doi:10.1007/s11430-016-9043-3

Xiao, W., Han, C., Yuan, C., Sun, M., Zhao, G., Shan, Y., et al. (2010). Transitions Among Mariana-, Japan-, Cordillera- and Alaska-type Arc Systems and Their Final Juxtapositions Leading to Accretionary and Collisional Orogenesis. *Geol. Soc. Lond. Spec. Publications* 338, 35–53. doi:10.1144/sp338.3

Yin, A. (2006). Cenozoic Tectonic Evolution of the Himalayan Orogen as Constrained by Along-Strike Variation of Structural Geometry, Exhumation History, and Foreland Sedimentation. *Earth-Science Rev.* 76 (1), 1–131. doi:10.1016/j.earscirev.2005.05.004

Yuan, H.-L., Gao, S., Dai, M.-N., Zong, C.-L., Günther, D., Fontaine, G. H., et al. (2008). Simultaneous Determinations of U-Pb Age, Hf Isotopes and Trace Element Compositions of Zircon by Excimer Laser-Ablation Quadrupole and Multiple-Collector ICP-MS. *Chem. Geology.* 247 (1), 100–118. doi:10.1016/j.chemgeo.2007.10.003

Conflict of Interest: The authors declare that the research was conducted in the absence of any commercial or financial relationships that could be construed as a potential conflict of interest.

Publisher's Note: All claims expressed in this article are solely those of the authors and do not necessarily represent those of their affiliated organizations, or those of the publisher, the editors, and the reviewers. Any product that may be evaluated in this article, or claim that may be made by its manufacturer, is not guaranteed or endorsed by the publisher.